4914–4928 *Nucleic Acids Research, 2023, Vol. 51, No. 10* *Published online 6 April 2023*
https://doi.org/10.1093/nar/gkad237

CTC1 OB-B interaction with TPP1 terminates telomerase and prevents telomere overextension

Huan Wang[1,2,†], Tengfei Ma[1,2,†], Xiaotong Zhang[2], Wei Chen[2], Yina Lan[2], Guotao Kuang[2], Shih-Jui Hsu[3], Zibin He[4], Yuxi Chen[4], Jason Stewart[5], Anukana Bhattacharjee[3], Zhenhua Luo[1,2,*], Carolyn Price[3,*] and Xuyang Feng[1,2,*]

[1]Department of Pediatrics, The First Affiliated Hospital, Sun Yat-sen University, Guangzhou, Guangdong, China, [2]Institute of Precision Medicine, The First Affiliated Hospital, Sun Yat-sen University, Guangzhou, Guangdong, China, [3]Department of Cancer Biology, University of Cincinnati, Cincinnati, OH, USA, [4]MOE Key Laboratory of Gene Function and Regulation, State Key Laboratory of Biocontrol, School of Life Sciences, Sun Yat-sen University, Guangzhou, Guangdong, China and [5]Department of Biological Sciences, University of South Carolina, Columbia, SC, USA

Received July 11, 2022; Revised March 16, 2023; Editorial Decision March 17, 2023; Accepted March 31, 2023

ABSTRACT

CST (CTC1-STN1-TEN1) is a telomere associated complex that binds ssDNA and is required for multiple steps in telomere replication, including termination of G-strand extension by telomerase and synthesis of the complementary C-strand. CST contains seven OB-folds which appear to mediate CST function by modulating CST binding to ssDNA and the ability of CST to recruit or engage partner proteins. However, the mechanism whereby CST achieves its various functions remains unclear. To address the mechanism, we generated a series of CTC1 mutants and studied their effect on CST binding to ssDNA and their ability to rescue CST function in *CTC1*$^{-/-}$ cells. We identified the OB-B domain as a key determinant of telomerase termination but not C-strand synthesis. CTC1-ΔB expression rescued C-strand fill-in, prevented telomeric DNA damage signaling and growth arrest. However, it caused progressive telomere elongation and the accumulation of telomerase at telomeres, indicating an inability to limit telomerase action. The CTC1-ΔB mutation greatly reduced CST-TPP1 interaction but only modestly affected ssDNA binding. OB-B point mutations also weakened TPP1 association, with the deficiency in TPP1 interaction tracking with an inability to limit telomerase action. Overall, our results indicate that CTC1-TPP1 interaction plays a key role in telomerase termination.

INTRODUCTION

Telomeres, the protective structures at the end of the liner chromosomes, are composed of the telomeric DNA and its associated proteins (1–3). Telomeric DNA contains a double-stranded DNA (dsDNA) region and a short single-stranded DNA (ssDNA) G-overhang at the 3' end of the G-strand (4). In human somatic cells, telomeres shorten every cell cycle due to an inability to replicate the DNA 5' terminus (the end replication problem). However, some cells, including stem cells have the ability to maintain their telomere length through telomerase-mediated elongation. Many cancer cells also survive telomere crisis by activating telomerase expression (5–7). In telomerase positive cells, the double stranded region of the telomere is replicated by the canonical replication machinery, telomerase is then recruited to add telomeric repeats to the end of the G-strand (8,9). The complementary C-strand is subsequently generated via a process called C-strand fill-in (9,10). DNA polymerase α-primase (Pol α) is proposed to carry out this C-strand synthesis.

The complex process of telomere replication is regulated by multiple telomere binding proteins (11). The most abundant human telomeric protein complex is shelterin, also called the telosome, which consists of TRF1, TRF2, RAP1, TIN2, TPP1, POT1 (12,13). TRF1 and TRF2 bind to the dsDNA, while POT1 binds to the G-overhang. TPP1 interacts with POT1 and enhances the affinity of POT1 for ssDNA. TIN2 works as a hub to bridge TRF1 and TRF2 to TPP1-POT1. CST (CTC1-STN1-TEN1) is a second protein complex that plays key roles in telomere replication (14,15). CST is a ssDNA binding complex, that binds to

*To whom correspondence should be addressed. Tel: +86 020 8760 6865; Email: fengxy58@mail.sysu.edu.cn
Correspondence may also be addressed to Carolyn Price. Email: carolyn.price@uc.edu
Correspondence may also be addressed to Zhenhua Luo. Email: luozhh35@mail.sysu.edu.cn
†The authors wish it to be known that, in their opinion, the first two authors should be regarded as Joint First Authors.
Present address: Anukana Bhattacharjee, Division of Biomedical Informatics, Cincinnati Children's Hospital Medical Center, Cincinnati, OH, USA.

G-overhangs and dsDNA-ssDNA junctions at telomeres via multiple OB (oligonucleotide/oligosaccharide-binding) domains. CST also communicates with TPP1-POT1 via the physical interaction of CTC1-TPP1, CTC1-POT1 and STN1-TPP1 (16).

Under conditions of homeostatic telomere length maintenance, human telomerase adds about 60 nt of DNA per cell cycle (17). This tightly regulated process is orchestrated by shelterin, telomerase and CST. Telomerase is recruited to telomeres through TPP1, which interacts with the telomerase protein subunit TERT (18,19). This interaction is mediated by the TEN and IFD domains on TERT and the TEL patch surface of OB-fold domain on TPP1 (20–23). The OB domain of TPP1 is not only essential for telomerase recruitment, but also functions in the stimulation of telomere processivity (defined as the number of telomeric repeats added on a single telomerase-primer binding event) (22,24). TPP1, together with POT1, enhances telomerase processivity *in vitro* by stabilizing the DNA, unfolding secondary structures on G-overhangs, preventing telomerase dissociation from telomeric DNA and by increasing the translocation of telomerase along the DNA (24–27). TIN2 also cooperates with TPP1-POT1 to recruit telomerase and to stimulate telomerase processivity (21,28–30). In contrast, CST functions to limit the number of repeats added by telomerase and mediates C-strand fill-in (16,31,32). However, the actual mechanisms of telomerase termination and C-strand fill-in are still unclear.

In vitro studies suggest several ways by which CST might limit telomerase action. These include sequestration of the extended G-overhangs to block continued telomerase activity, or through disruption of further telomerase recruitment by TPP1-POT1 (33). Our previous work revealed that TEN1 deletion decreases the affinity and stability of CTC1-STN1 (CS) binding to ssDNA and causes a deficiency in C-strand fill-in (34). However, despite the reduced DNA binding ability, CS could still terminate telomerase action. Additional studies by Zaug *et al.* indicated that CST is unable to evict elongating telomerase (33). These results imply that simple competition with telomerase for G-overhang binding may not be sufficient to prevent telomere extension, suggesting a more complex mechanism is used for telomerase termination.

A recent cryo-EM (cryo-electron microscopy) structure of CST revealed seven tandem OB domains (OB-A to G) within CTC1, with the C-terminal domains (OB-D through OB-G) acting as a hub for STN1 interaction and DNA binding (35). Several mutations in the OB domains of CTC1 cause the 'inherited telomere syndrome' Coats plus (35–38). Mutations located close to the C terminal binding hub weaken binding to STN1 (L1142H) or affinity for single stranded telomeric substrates (R975G, C985Δ and R987W) (37,39,40). The other OB domains within this hub (OB-folds on STN1 and TEN1) are also important for telomeric DNA binding (41). Meanwhile, N-terminal mutations (A227V, V259M and V665G) disrupt interaction between CTC1 and Pol α (38). These findings suggest that each OB-fold domain mediates different protein/DNA associations, and thus different aspects of CST function. However, the contributions of each OB-fold to CST function remain to be assessed.

Structural comparisons indicate that CST has similarities to replication protein A (RPA), a heterotrimeric ssDNA binding complex that regulates many aspects of DNA metabolism. RPA engages DNA through multiple OB-folds and its capacity to direct DNA replication and repair reactions stems from the ability of these OB domains to bind and release DNA independently without causing dissociation of the entire complex (42). The resulting dynamic binding allows RPA to diffuse along DNA, displace bound proteins, and to engage other proteins on the DNA. The structural similarity between CST and RPA indicates that CST may use a similar dynamic binding mechanism to regulate the association of partner proteins with DNA; e.g. Pol α and telomerase. This model may explain how the altered DNA binding caused by loss of TEN1 or mutation of CTC1 could disrupt C-strand fill-in or other CST functions (17,34,38,39).

Since the OB-folds in CTC1 are fundamental to CST function, we set out to determine how individual OB-folds contribute to specific aspects of telomere replication. We constructed a series of OB domain deletion mutants and assessed their effects on DNA binding, C-strand fill-in and telomerase regulation. We show that CTC1 OB-B domain directs telomerase termination and pinpoint the interaction between CTC1 and TPP1 as being key to this process.

MATERIALS AND METHODS

Cell culture and generation of CTC1 mutation cells

HCT116 cells were grown in McCoy's medium and HEK293T cells were grown in DMEM, supplemented with 10% FBS and antibiotics. Sf9 cells were cultured in Grace' Insect Medium (Gibco) containing 10% inactivated FBS. HCT116 cells with conditional *CTC1* disruption were described previously (32). To introduce wild-type or mutant Flag-CTC1, retrovirus was generated by co-transfecting HEK293T cells with pMIEG3 vector encoding wild-type or mutant Flag-CTC1, gag-pol and env. Viral supernatant was used to infect HCT116 $CTC1^{F/F}$ cells and the cells were then selected by flow cytometry for GFP expression.

Co-immunoprecipitation (co-IP) and western blotting

Cells were lysed in NP-40 lysis buffer (20 mM Tris pH 8.0, 100 mM NaCl, 1 mM $MgCl_2$ and 0.1% Igepal). For immunoprecipitation, each sample was incubated with Flag M2 beads (Sigma) at 4°C for 2 hrs to 16 hrs, washed with NP-40 lysis buffer and boiled in 2 × SDS loading buffer. Samples were separated by SDS-PAGE and transferred to nitrocellulose membranes. The membranes were blocked with 5% milk in TBS-Tween (0.1% Tween-20) and incubated with antibodies to Flag (Sigma), Myc (Abcam), HA (Cell Signaling Technology), actin (Bioss), actinin (Santa Cruz), Pol α (Bethyl), GST (Cell Signaling Technology), POT1 (homemade) and STN1(homemade).

Chromatin immunoprecipitation (ChIP)

ChIP was performed as previously described (43). Cells were fixed with 1% formaldehyde, treated with 200 mM glycine, pelleted by centrifugation, suspended in swelling

buffer (25 mM HEPES pH 7.9, 10 mM KCl, 1.5 mM $MgCl_2$, 1 mM EDTA, 1 mM DTT, 0.25% Triton X-100 and protease inhibitors), incubated in sonication buffer (50 mM HEPES pH 7.9, 150 mM NaCl, 1 mM EDTA, 0.1% Sodium deoxycholate, 0.1% SDS, 1% Triton X-100 and protease inhibitors) and sonicated for 20 min. For immunoprecipitation, samples containing supernatant (0.3 mg protein), antibody (3 μg Flag M2, Sigma A2220) and 20 μg bacterial DNA were incubated overnight at 4°C. Protein A/G PLUS agarose beads (Santa Cruz) were added to samples for 1 hr, then washed and eluted in 450 μl elution buffer (1% SDS, 0.1 M $NaHCO_3$). Cross-linking was reversed by incubation at 65°C overnight. The eluate was brought to 10 mM EDTA, 40 mM Tris-HCL pH 6.8 and treated with 5 μg RNase A, 40 μg protease K and purified by phenol-chloroform extraction. Samples were analyzed by slot blot hybridization with $(TA_2C_3)_3$ probe and quantified by Phosphorimager. The background from the no antibody control was subtracted and the amount of precipitated DNA was calculated as a percentage of the corresponding input.

Protein purification

HEK293T cells were co-transfected with Flag-CTC1, Flag-STN1 and TEN1 using PEI (polyethyleneimine) for 72 hrs. Cells were lysed with NP-40 lysis buffer (0.1% Igepal, 20 mM Tris–HCl pH 8.0, 100 mM NaCl, 1 mM $MgCl_2$, and protease inhibitors). The supernatant was incubated with Flag-M2 beads for 2 h. Then, the beads were washed and eluted with 3 × Flag peptides. The protein concentration was quantified by silver staining.

For baculovirus expression, Sf9 cells in suspension were infected with baculovirus expressing Flag-CTC1 or GST-TPP1-POT1, and grown in a 500 ml shaker flask at 130 rpm for 72 h at 27°C. The infected cells were harvested by centrifugation at 800 g for 10 min, and washed once using PBS. The cell pellets were stored at -80°C or lysed with lysis buffer (50 mM Tris–HCl pH 8.0, 300 mM NaCl) containing protease inhibitors, and sonicated for 4 times (2 s on/4 s off). After centrifugation at 15 000 g for 10 min, the supernatant was incubated with GST beads for 1 hr. Then, the beads were eluted with elution buffer (50 mM Tris–HCl pH 8.0, 300 mM NaCl, 10 mM reduced glutathione, and proteinase inhibitors). The sample was desalted, concentrated into the lysis buffer without glutathione, and stored at –20°C with equal volume of glycerol.

Electrophoretic gel mobility shift assays (EMSAs)

EMSAs were performed as previously described (44). Briefly, the indicated amounts of protein complex were incubated with 0.1 nM ^{32}P-labeled (or CY7-labeled) oligonucleotide in 25 mM Tris–HCl pH 8.0, 100 mM NaCl, 1 mM DTT for 30 min at RT. For *Kd* analysis, protein was incubated with 0.01 nM ^{32}P-labeled oligonucleotide in 25 mM Tris–HCl pH 8.0, 100 mM NaCl, 1 mM DTT for 18 hrs at 4°C. Samples were separated in 0.7% agarose gels with 1 × TAE and quantified by Phosphorimaging. To determine *Kd(app)*, the amount of bound versus free DNA was quantified using ImageQuantTL software. Data were fit to a one site specific saturation binding equation using GraphPad Prism software. The oligonucleotides used were Tel-18 (5′-GGTTAG GGTTAG GGTTAG), Tel-36 (5′-GGTTAG GGTTAG GGTTAG GGTTAG GGTTAG GGTTAG) and NonTel-48 (5′-AGCGTATCCGTTCAG TTGAGCGTATCCGTTCAGTTGAGCGTATCCGTT).

In vitro pull-down

Sf9 cells expressing Flag-CTC1 were lysed with NP-40 lysis buffer containing protease inhibitors and sonicated 4 times (2 s on/ 4 s off). After centrifugation at 15 000 g for 10 min, the supernatant was incubated with Flag-M2 beads for 2 h at 4°C. Purified GST-TPP1-POT1 was added and incubated with for another 1 h at 4°C. After washing with 1 mL NP-40 lysis buffer and centrifugation for 6 times, the precipitate was saved as the pull-down product.

Growth curve

Growth curves were performed as previously described (32), with three repetitions for each cell line.

TIF (telomere induced foci) analysis

Cells grown on coverslips were fixed with 4% paraformaldehyde, permeabilized with 0.5% Triton X-100, blocked with 5% goat serum and incubated in antibody to γH2AX. After secondary antibodies incubation, cells were fixed again and hybridized with TelC-Alexa488 PNA probes (5′-CCCTAACCCTAACCCTAA, Biosynthesis). Images were taken with a Zeiss fluorescence microscope.

TRF (terminal restriction fragments) and G-overhang analysis

TRF and G-overhang analysis were performed as previously described (32,45). Briefly, genomic DNA was digested overnight with HinfI, MspI, and RsaI (control samples were treated with ExoI for 48 hrs prior to restriction digestion), then separated in agarose gels; 0.7% agarose for TRF and 1% for G-overhang analysis. The gels were dried, denatured (initially hybridized with under non-denaturing conditions for G-overhang analysis) and hybridized with ^{32}P-labeled $(TA_2C_3)_3$ probe.

Signals were detected and quantified by PhosphorImager. For TRFs, the mean telomere length was determined as described previously (46). Briefly, each lane was divided into 100 boxes using Image Quant software and calculated by applying the formula Sig/ (SigI/LI), where Sig is the sum of the signal from all 100 boxes, SigI is the signal in an individual box, and LI corresponds to the average length of the DNA in that box as determined using DNA markers and a standard curve.

Telomere FISH

FISH was performed on MeOH/acetic acid fixed metaphase spreads as previously described (32,47). TelC-Alexa488 PNA G-strand probes (5′-CCCTAACCCTAACCCTAA) or TelG-Cy3 PNA C-strand probes (5′-GGGTTAGGGTTAGGGTTA, Biosynthesis) were used to label telomeres. Images were taken at a

constant exposure time. For quantitative measurement of telomere length (Q-FISH), telomere fluorescence intensity was integrated using the TFL-TELO program.

RNA FISH

hTERT and hTR were both overexpressed in cells before preforming the experiments. Cells on coverslips were fixed with 3.6% paraformaldehyde and 10% acetic acid, permeabilized with 0.5% Triton X-100, blocked with 3% goat serum and 0.1% BSA, incubated in anti-TRF1 antibodies. After secondary antibody incubation, cells were fixed again with 70% ethanol and hybridized with FITC labeled (*, star marks in the sequence below) TERC probe mix (TAKARA). For telomere FISH following RNA FISH, TelG-Cy3 PNA C-strand probes were used to hybridize telomeric DNA followed TERC signal fixation in 70% ethanol for slides without TRF1 antibodies incubation. Images were taken with an Olympus fluorescence microscope.

Probe1 (against hTR 128–189 nt):

- 5′-GC∗GACATTTT∗TGTTTGCTC∗AGAATGAAC GG∗GGAAGGCGGCAGGCCGAGGC∗T

Probe 2 (against hTR 331–383 nt):

- 5′-C∗CCGTTCCTCTTCC∗GCGGCCTGAAAGGCC ∗GAACCTCGCCC∗CGCCCCCGAG∗G

Probe 3 (against hTR 393–449 nt):

- 5′-A∗GTGTGAGCCGAG∗CCTGGGTGCACG∗CCC ACAGCTCAGGGAA∗CGCGCCGCGC∗C

Immunoprecipitation quantitative TRAP (IP-QTRAP) assay

HEK293T cells stable expressing TPP1-Flag and transient transfected with different amount of HA-CTC1 or HCT116 *CTC1*$^{F/F}$ cells stable expressing TPP1-Flag were used. Cells were lysed with RNase-free NETN lysis buffer (40 mM Tris–HCl pH 8.0, 100 mM NaCl, 0.5% Igepal, 1 mM EDTA and 10% glycerol). For immunoprecipitation, each sample was incubated with Flag M2 beads (Sigma) at 4°C for 2 hrs, washed with NETN lysis buffer and eluted with elution buffer (25 mM Tris–HCl pH 7.4, 136 mM NaCl, 2.6 mM KCl, 1 mM $MgCl_2$, 1 mM EGTA, 10% glycerol, 1 mM DTT, proteinase inhibitor and RNase inhibitor) 3 times. QTRAP was performed with 2 × GoTaq qPCR master mix (Promega), CXR Reference Dye, 10 mM EGTA, 100 ng/μl TS primer (5′-AATCCGTCGAGCAGAGTT) and 100 ng/μl ACX primer (5′-GCGCGGCTTACCCTTACCCTTACCCTAACC) using an Applied Biosystems real-time PCR system.

CST-pol α structure image

CST- Pol α cyto-EM structure was downloaded from the study of He *et al.* (48). A227 and V259 were mapped onto the CST- Pol α structure using Mol* on RCSB PDB web site (49).

Statistical methods

Data from a minimum of three experiments were analyzed by two-tailed Student's *t* test. *P*-values: $*P < 0.05$, $**P < 0.01$).

RESULTS

Effect of CTC1 OB-fold deletions on CST complex formation and DNA binding

To dissect the molecular functions of the OB-fold domains in CTC1, we generated seven deletion mutations designed to disrupt one or more of the OB folds. Their nomenclature refers to the corresponding OB-folds identified in the recent CST cryo-EM structure (35) (Figure 1A). To determine how the mutations affect CST complex formation and interaction with DNA Pol α, we performed co-immunoprecipitation experiments using extracts from HEK293T cells transiently expressing Flag-tagged CTC1. We found the C-terminal OB deletion mutants (ΔF-G and ΔG) lost interaction with STN1 (Figure 1B), which was consistent with previous findings of a strong interaction between CTC1 OB-G and the OB-fold domain on STN1 (35). Interestingly, while ΔF-G and ΔG co-immunoprecipitated Pol α as efficiently as WT CTC1, this was reduced for ΔA and ΔB (Figure 1B) even though the recent cryo-EM structures showed that Pol α associates with CST at C-S-T interaction hub located at the C-terminus of CTC1(48, 50). The large reduction in Pol α co-immunoprecipitation with ΔB is consistent with previous findings showing that point mutations in OB-B disrupt Pol α interaction (38), indicating that CTC1 likely has a second N-terminal interaction site for Pol α that does not involve STN1/TEN1.

To investigate the effects of CTC1 OB-fold deletion on telomere binding, we performed chromatin immunoprecipitation (ChIP) to monitor telomere localization. Flag-tagged CTC1 wild-type (WT) or mutant protein was stably expressed in *CTC1* conditional knockout HCT116 cells, where endogenous *CTC1* was deleted (Supplementary Figure S1A, B). Since interaction with Pol α is important for CST localization to the nucleus, a nuclear localization signal (NLS) was added to the N-terminus of CTC1 to avoid potential localization issues (38). Strikingly, ΔB was the only mutant that immunoprecipitated significant levels of telomeric DNA (Figure 1C), although its immunoprecipitation efficiency was about half that of WT-CTC1. The lack of telomere association by ΔD and ΔE-F fits with previous findings by us and others that interaction between CTC1 and STN1 is required for CTC1 telomere localization (34,37,38) and that OB-D through OB-G form a hub for STN1 interaction and DNA binding (35). However, the lack of telomere association by ΔA and ΔC was unexpected and suggests that these OB domains may play a more direct role in telomere localization.

We next examined how the OB-fold mutations affected DNA binding activity by performing electrophoretic mobility shift assays (EMSAs) with CST purified from HEK293T cells transiently transfected with WT or mutant CTC1, STN1 and TEN1 (Supplementary Figure S1C). In these assays, DNA oligos were incubated with purified protein

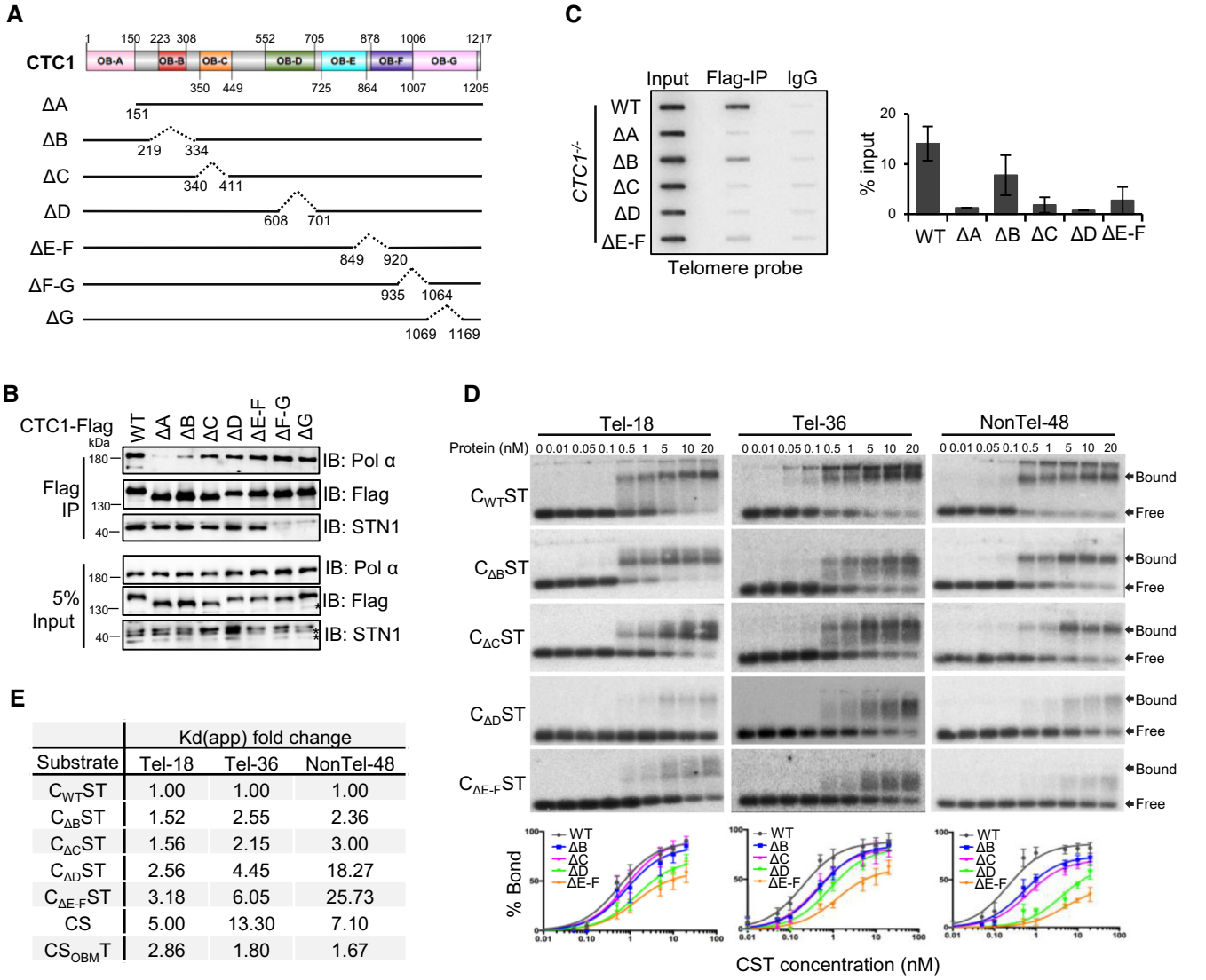

E

	Kd(app) fold change		
Substrate	Tel-18	Tel-36	NonTel-48
$C_{WT}ST$	1.00	1.00	1.00
$C_{\Delta B}ST$	1.52	2.55	2.36
$C_{\Delta C}ST$	1.56	2.15	3.00
$C_{\Delta D}ST$	2.56	4.45	18.27
$C_{\Delta E\text{-}F}ST$	3.18	6.05	25.73
CS	5.00	13.30	7.10
$CS_{OBM}T$	2.86	1.80	1.67

Figure 1. Effect of CTC1 OB-fold deletions on CST complex formation and DNA binding. (**A**) Cartoon showing the design of CTC1 mutants. (**B**) Immunoprecipitation of CTC1 mutants with STN1 and Pol α. FLAG-tagged CTC1 was precipitated from HEK293T cell lysates using Flag M2 beads. Western blots were performed with antibodies to Flag, STN1 or Pol α. *, cross-reacting bands. (**C**) ChIP analysis showing the localization of wild-type (WT) and mutant CTC1 to telomeres. Lower panel shows quantification data. $N \geq 3$ independent experiments, Error bars indicate mean ± S.E.M. *CTC1*$^{-/-}$ cells expressing Flag-tagged WT or mutant CTC1 were grown with tamoxifen for 7 days. (**D**) EMSAs showing WT and mutant CST binding to 18 or 36 nt telomeric G-strand (Tel-18, Tel-36) or 48 nt non-telomeric (NonTel-48) ssDNA substrates (upper). Reactions contained 0.1 nM DNA and the indicated concentrations of protein. The corresponding plots (lower) used to calculate Kd(apps). $N \geq 3$ independent experiments. (**E**) *Kd(app)* fold change for mutant CST binding to the indicated substrates relative to $C_{WT}ST$.

and gel electrophoresis was used to separate residual free DNA from the slower migrating protein bound oligos. The ΔD and ΔE-F deletions caused the expected large decrease in DNA binding, as indicated by disappearance of the intense bands corresponding to stable CST-DNA complexes and accumulation of unshifted DNA or a smear corresponding to more transient DNA-protein complexes (Figure 1D and Supplementary Figure S1D). However, complexes with the N-terminal CTC1 OB-fold deletions $C_{\Delta B}ST$ and $C_{\Delta C}ST$ bound both telomeric (Tel-18 and Tel-36) and non-telomeric (NonTel-48) substrates with only modestly lower efficiency than $C_{WT}ST$. Binding experiments were not performed with the ΔA mutant as we were unable to obtain stable $C_{\Delta A}ST$ complex. To obtain a more quantitative comparison of mutant and WT CST binding, we determined the *Kd(app)* by calculating the amount of bound DNA versus free DNA in each lane (Figure 1D and Supplementary Figure S1E). The *Kds* revealed only a 1.5–3 fold reduction in $C_{\Delta B}ST$ and $C_{\Delta C}ST$ binding affinity relative to that of $C_{WT}ST$ (Figure 1E). Since $C_{\Delta C}ST$ bound DNA with similar affinity to $C_{\Delta B}ST$, but failed to localize to telomeres, we questioned whether ΔC had altered the architecture of the CST heterotrimer and hence its ability to oligomerize (35). To test for oligomerization, we transfected HEK293T cells with Flag and HA-tagged CTC1 constructs and looked for co-immunoprecipitation. Flag tagged-CTC1 WT, ΔB, ΔC and ΔD were all able to IP the matching HA-tagged CTC1 (Supplementary Figure S1F), ruling out the possibility that

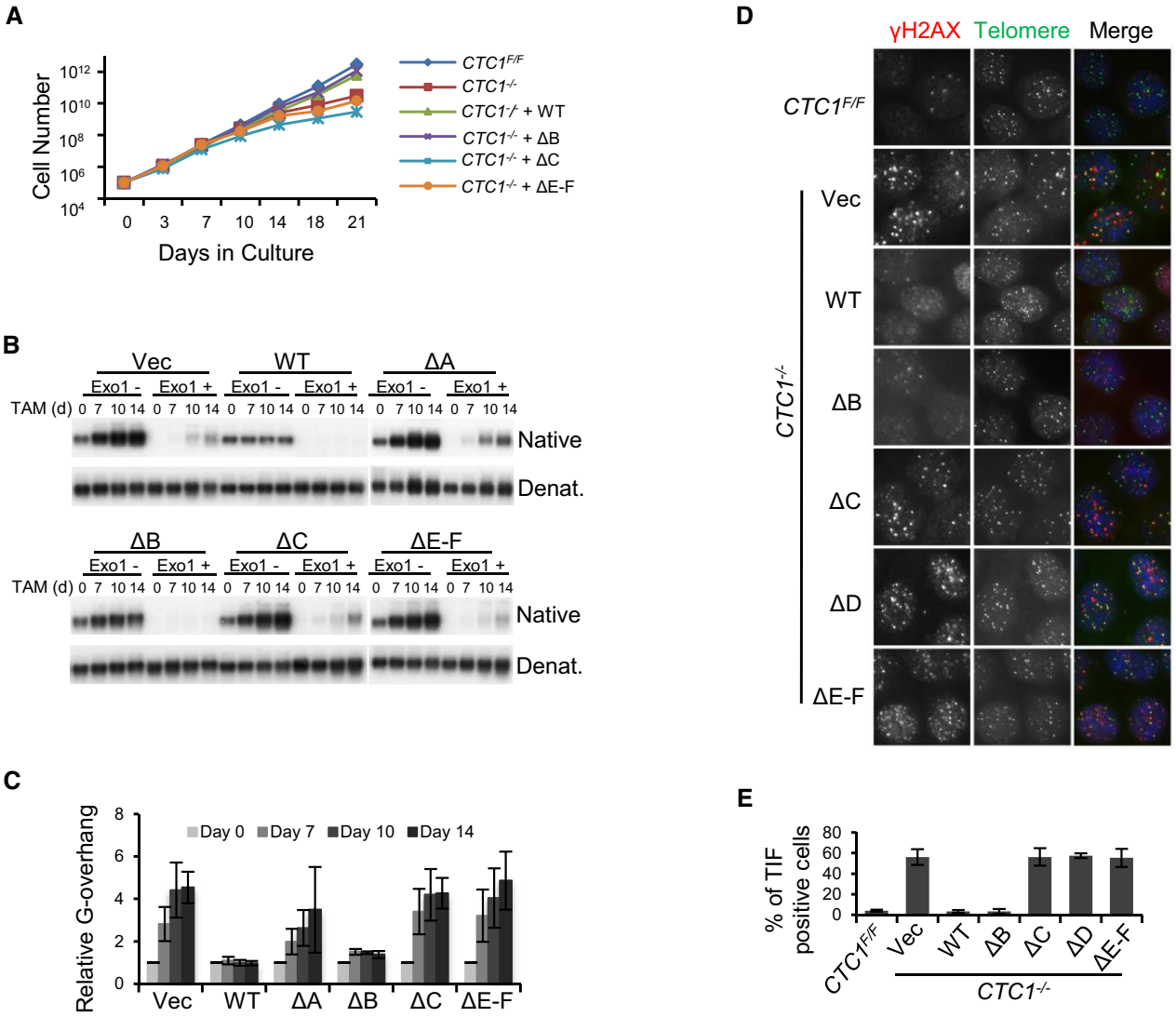

Figure 2. CTC1-ΔB rescues the growth defect, C-strand fill-in deficiency and telomeric DNA damage caused by *CTC1* disruption. (**A**) Representative growth curves showing proliferation of *CTC1* conditional knockout cells expressing empty vector, WT or mutant CTC1 at the indicated times after tamoxifen (TAM) addition to induce endogenous *CTC1* gene disruption. (**B**) G-overhang abundance in *CTC1* conditional knockout cells expressing WT or mutant CTC1 following the indicated times of TAM treatment. Gels show in-gel hybridization of TAA(C_3TA_2)$_3$ probe to genomic DNA with/without Exo1 treatment. (**C**) Quantification of relative G-overhang abundance. Overhang abundance in $CTC1^{-/-}$ cells was normalized to that of $CTC1^{F/F}$ cells (i.e. $t = 0$). $N = 3$ independent experiments, Error bars indicate mean ± S.E.M. (**D**) Representative images of TIFs in the indicated cells. Telomeres were detected by FISH (green), γH2AX by immunostaining (red), chromosomes are counterstained with DAPI (blue). (**E**) Quantification of cells in (D) with ≥ 3 TIFs. Error bars indicate mean ± S.E.M.

defective oligomer formation is responsible for the failure of ΔC to localize to telomeres.

CTC1-ΔB rescues the growth defect, C-strand fill-in deficiency and telomeric DNA damage caused by *CTC1* disruption

To assess the effects of the CTC1 OB-fold deletions *in vivo*, we first asked whether expression of mutant protein rescued the decline in proliferation that is normally observed in HCT116 cells over a 3-week period following induction of *CTC1* gene disruption (32). A similar proliferation defect was observed in $CTC1^{-/-}$ cells expressing only the empty vector and cells expressing the ΔC and ΔE-F mutants (Figure 2A). In contrast, expression of CTC1-WT and ΔB fully rescued the growth defect.

The decline in cell growth of $CTC1^{-/-}$ cells is at least partially caused by the generation of extremely long G-overhangs that induce DNA damage signaling (32). We therefore examined G-overhang length by performing non-denaturing in-gel hybridization of telomere probes to genomic DNA to detect ssDNA. As with rescue of the growth defect, only WT-CTC1 and ΔB prevented the continued G-overhang elongation normally observed after CTC1 loss (Figure 2B-C and Supplementary Figure S1G). Cells expressing ΔB did exhibit a slight increase in basal overhang

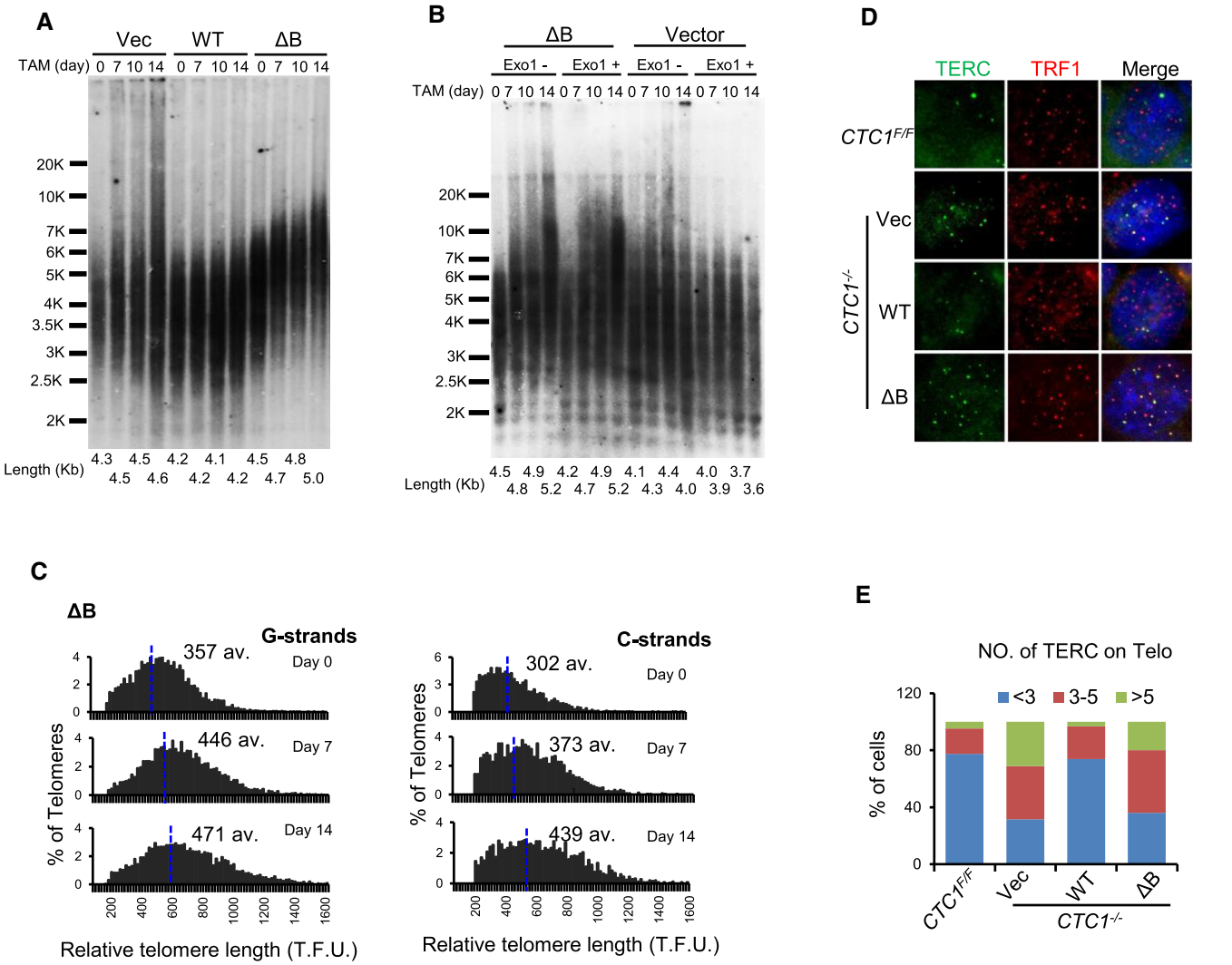

Figure 3. CTC1 OB-B domain is essential for telomerase termination. (**A**, **B**) Southern hybridization showing TRFs from *CTC1* conditional knockout cells expressing vector or mutant CTC1 and treated with TAM for the indicated times. Gels were hybridized with TAA$(C_3TA_2)_3$ probe. Mean telomere length is indicated below each lane. (A) TRFs in *CTC1* conditional knockout cells expressing empty vector, CTC1 WT, ΔB. (B) TRFs from cells expressing ΔB or empty vector with/without treatment of genomic DNA with Exo1. (**C**) Analysis of telomere length by Q-FISH in CTC1-ΔB expressing cells. Metaphase spreads were hybridized with $(C_3TA_2)_3$ G-strand probe (left panel) or $(G_3AT_2)_3$ C-strand probe (right panel). Histograms show distribution of relative telomere lengths expressed as fluorescence intensity (TFU, telomere fluorescence unit). A minimum of 100 TFU was set as the cut-off. av.; median value, also shown by blue line. >2000 telomeres quantified per sample. (**D**) Representative images showing telomere localization of TERC. Telomeres detected by immunostaining of TRF1 (red), TERC by FISH (green), chromosomes by DAPI (blue). (**E**) Quantification of cells with TERC-TRF1 co-localization foci. >200 cells quantified per sample. $N = 3$ independent experiments.

length, which might reflect the decreased CST telomere localization.

The growth defect in *CTC1*$^{-/-}$ cells is due to the long G-overhangs eliciting DNA damage signaling (32). Thus, normal growth and lack of continued G-overhang elongation in cells expressing CTC1-ΔB implied that the telomeres were not being detected as DNA damage. To test this supposition, we looked for telomeric γH2AX staining using IF-FISH. As anticipated, we found that ΔB fully rescued TIF (telomere dysfunction induced foci) formation in *CTC1*$^{-/-}$ cells (Figure 2D, E). However, the ΔC, ΔD and ΔE-F mutants, which failed to rescue cell proliferation and G-overhang elongation, also failed to prevent TIFs. It is notable that, despite the interaction between ΔB and Pol α being greatly decreased (Figure 1B), the CTC1-ΔB mutant is still capable of largely rescuing G-overhang elongation. This finding implied that stable interaction with Pol α may not be required for CST to function in C-strand fill-in.

CTC1 OB-B domain is essential for telomerase termination

We then examined the influence of the OB-fold mutants on telomere length. In initial experiments, we used in gel hybridization to visualize changes in terminal restriction fragment (TRF) length over a two-week period. As previously observed, *CTC1* disruption led to the accumulation of much longer TRFs between days 7–10 (Figure 3A). We previously showed that this increase in TRF length arises from

overextension of the telomeric G-strand by unterminated telomerase. Expression of WT-CTC1 in *CTC1*$^{-/-}$ cells prevented accumulation of the longer TRFs (Figure 3A). In contrast, expression of ΔC, ΔE-F and 1196-Δ7 (a seven amino acids deletion that disrupts interaction with STN1) (38) resulted in a generally similar lengthening pattern to the vector only control (Supplementary Figure S2A, B). Intriguingly, ΔB expression resulted in continuous telomere elongation with a tighter banding pattern than that observed for the vector control.

Despite the increase in G-strand length in *CTC1*$^{-/-}$ cells, the lack of C-strand fill-in simultaneously leads to net shortening of the telomere duplex (32). This shortening of the DNA duplex can be observed as a gradual decline in average TRF length after the extended ssDNA G-overhangs are removed by treatment with Exonuclease 1 (Exo1) (Figure 3B and Supplementary Figure S2B, C) (32). We saw a similar decline in average TRF length with ΔE-F after Exo 1 treatment and a partial decline in ΔC. However, while Exo1 treatment of DNA from ΔB expressing cells reduced the longest telomere signals, the TRFs continued to exhibit a progressive increase in length over time in culture (Figure 3B and Supplementary Figure S2C). This finding suggests that CTC1-ΔB expression causes the double-stranded region of the telomere to be elongated rather than shortened.

To verify elongation of the telomere duplex DNA, we performed Q-FISH to detect the length of the G and C strands separately. Quantification of the data revealed both C-strand and G-strand lengthening in the ΔB expressing cells (Figure 3C), whereas the vector only control cells exhibited lengthening of G-strands and shortening of C-strands, and WT CTC1 largely rescued both G-strand lengthening and C-strand shortening, as previously observed (Supplementary Figure S2D) (32).

The rescue of telomere shortening but not lengthening by ΔB expression in *CTC1*$^{-/-}$ cells suggests that OB-B in CTC1 is necessary to prevent telomere lengthening but may not be required for C-strand fill-in. Since CST normally limits G-strand synthesis by telomerase, this finding suggested that ΔB might allow excess telomerase to accumulate on telomeres to allow additional rounds of DNA synthesis. To address this possibility, we used TERC RNA-FISH to examine whether the telomere localization of telomerase was affected by ΔB expression. To detect TERC at telomeres, hTR and hTERT were transiently overexpressed prior to performing the RNA-FISH. While the fraction of cells showing TERC at telomeres was partially affected by transfection efficiency, we reproducibly saw a large increase in TERC and TRF1 co-localization (TERC-positive telomere foci) in *CTC1*$^{-/-}$ and CTC1-ΔB expressing cells. On average, only ∼20% of *CTC1*$^{F/F}$ and *CTC1*$^{-/-}$ rescue cells (cells expressing WT CTC1) displayed >3 TERC-positive telomere foci per nuclei while ∼80% of *CTC1*$^{-/-}$ and CTC1-ΔB expressing cells displayed > 3 TERC-TRF1 foci per nucleus (Figure 3D-E). In our system, this result supports our conclusion that the CTC1 OB-B domain is necessary for CST to terminate telomerase activity and indicates that in our conditional CTC1 knockout system, this occurs by limiting telomerase accumulation at the telomere.

The above data demonstrating that ΔB fails to terminate telomerase activity and has a lower affinity for ssDNA than WT CST, fits with a sequestration model for telomerase termination where CST out-competes telomerase for binding to the G-overhang. However, our previous finding that CTC/STN1 (CS) complexes are fully functional for telomerase termination (34) indicate that the sequestration model is insufficient because CS has a substantially lower affinity for telomeric G-strand DNA than $C_{\Delta B}ST$ (CS complexes show a 5–13 fold decrease in K_d relative to WT CST, while $C_{\Delta B}ST$ show a 1.5–2.5 fold decrease in *Kd*, Figure 1E). Thus, taken together our findings imply that reduced G-overhang binding by $C_{\Delta B}ST$ is unlikely to be the only factor accounting for the deficiency in telomerase termination.

CTC1 OB-B domain deletion impairs CTC1-TPP1 interaction

Since CST and telomerase both interact with the shelterin subunit TPP1, CST binding to TPP1 has the potential to limit telomerase activity by interfering with the TPP-POT1-mediated enhancement of telomerase action (16). Thus, given that $C_{\Delta B}ST$ fails to limit telomerase action, we next examined whether the ΔB mutation somehow disrupts the CST-TPP1 interaction. We first performed co-IPs using extracts from HEK293T cells expressing tagged TPP1 and WT or mutant CTC1 and observed a significant decrease in TPP1-CTC1-ΔB association (Figure 4A and Supplementary Figure S3A). To examine the direct interaction between CTC1 and TPP1, we performed *in vitro* pull-down experiments with purified CTC1 WT or ΔB and TPP1-POT1 from insect Sf9 cells. These experiments showed that the physical interaction between ΔB and TPP1-POT1 was reduced (Figure 4B and Supplementary Figure S3B). Since CTC1 and STN1 both interact with TPP1 directly (16), we next examined whether the CTC1-STN1 interaction is important for CTC1-TPP1 association by performing co-IPs using STN1 truncation mutants (Supplementary Figure S3C) which have different binding affinity to CTC1, and the CTC1 1196-Δ7 mutant which is unable to bind to STN1 (35,38). We found that deletion of the STN1 N-terminal CTC1 binding domain disrupted TPP1 interaction as expected (51) but STN1-TPP1 interaction was unaffected by deletion of the C-terminal winged helix domain (Supplementary Figure S3D). The 1196-Δ7 mutant also interacted normally with TPP1 and the 1196-Δ7/ΔB double mutant showed a similar decrease in TPP1-interaction to the ΔB single mutant (Figure 4C), indicating that CTC1 can interact with TPP1 in the absence of STN1. Since it has been reported that TPP1 phosphorylation is important for telomerase recruitment, we used co-immunoprecipitation experiments to test whether CTC1 WT or ΔB mutant preferentially interacted with phosphorylated TPP1. Nocodazole was used to synchronize the cells to G2/M phase in order to visualize the phosphorylated TPP1 (52). Our results indicated that CTC1 WT interacted with both phosphorylated and non-phosphorylated TPP1 and CTC1-ΔB had reduced interaction with both forms (Figure 4D).

To further investigate the CTC1-TPP1 interaction, we sought to identify the CTC1 interaction site on TPP1. TPP1 deletion mutations were made that corresponded to the reported telomerase, POT1 and TIN2 binding domains (Fig-

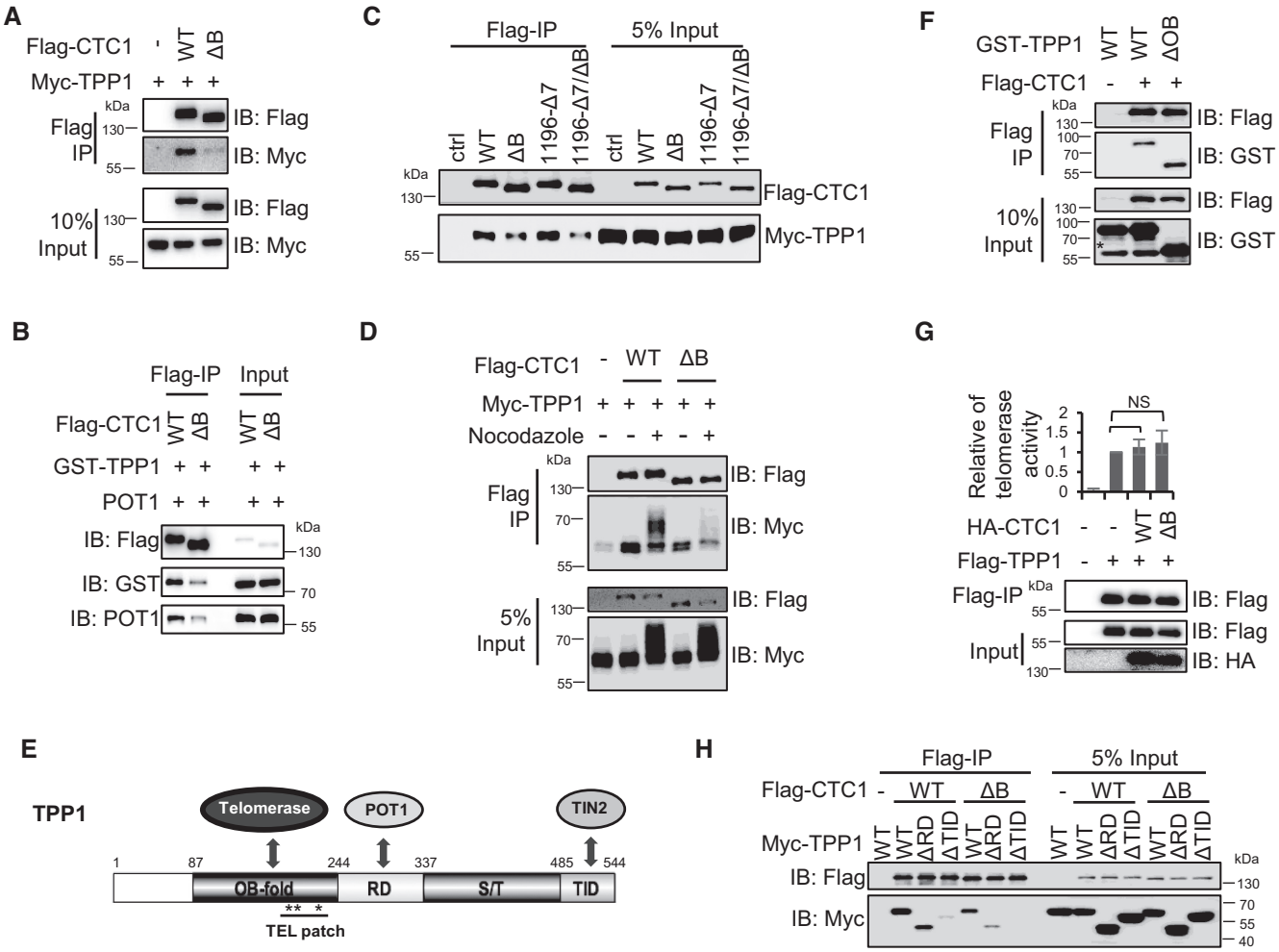

Figure 4. CTC1 OB-B domain deletion impairs CTC1-TPP1 interaction. (**A**, **C**, **D**) Immunoprecipitation of Flag-tagged CTC1 WT or indicated mutants with Myc-tagged TPP1 from HEK293T cell extracts. FLAG-tagged proteins were precipitated using Flag M2 beads. Nocodazole is added to synchronize the cells to G2/M phase in order to visualize the phosphorylated TPP1, the smeared signals on the top of TPP1 bands in (D). (**B**) *In vitro* pull-down of purified Flag-tagged CTC1 WT or ΔB with GST-tagged TPP1 and POT1 from Sf9 cells. (**E**) Schematic diagram of TPP1 domains and protein binding sites. *, telomerase binding sites on TEL patch. (**F**) Immunoprecipitation of Flag-tagged CTC1 with GST-tagged TPP1 WT or TPP1 ΔOB mutant. *, cross-reacting bands. (**G**) IP-QTRAP of Flag-tagged TPP1 from HEK293T extracts in the absence or presence of over-expressed CTC1 WT or ΔB. Upper panel shows quantification of QTRAP, and lower panel shows the western blot of IP. (**H**) Immunoprecipitation of Flag-tagged CTC1 with Myc-tagged TPP1 WT, ΔRD or ΔTID mutants.

ure 4E) (18,19,53). Co-IP of Flag-tagged CTC1 from cells also expressing truncated Myc-tagged TPP1 showed that deletion of the TPP1 OB domain (the hTERT binding domain) did not affect the CTC1-TPP1 interaction (Figure 4F), which was consistent with the data of Chen *et al.* (16). Mutations of the TEL-patch domain, the telomerase interaction surface of the TPP1 OB domain (22), also did not affect TPP1-CTC1 association (Supplementary Figure S3E), suggesting that CTC1 does not compete with telomerase for binding to TPP1. Consistent with this observation, telomerase activity assays indicated that neither CTC1-WT or ΔB expression, nor *CTC1* knockout, affected TPP1-hTERT interaction or telomerase recruitment by TPP1 (Figure 4G and Supplementary Figure S3F–I). However, we found that TPP1 RD domain (POT1 binding site) deletion weakened TPP1-CTC1 or TPP1-STN1 association and the TID domain (TIN2 binding site) deletion lost most of the interaction with CTC1/STN1 (Figure 4H and Supplementary Figure S3J). To narrow down the interaction site on the TID domain, we made a series of 4 residue deletion mutations and assayed for reduced CTC1 interaction by co-immunoprecipitation. These experiments indicated that residues 486–550 are most like the binding site for CTC1 (Supplementary Figure S3K).

As TPP1 associates with telomeres through interaction with TIN2 and POT1 (54,55), we questioned whether CTC1 might regulate TPP1 telomere localization by disrupting its association with these two shelterin proteins. However, overexpression of CTC1-WT or ΔB had no effect on TPP1-TIN2 or TPP1-POT1 association (Supplementary Figure S3L, M), suggesting that CTC1 can interact with TPP1 even when TPP1 is associated with TIN2 and POT1. Additionally, *CTC1* deletion did not affect the telomere localization of TPP1 or POT1 by ChIP (Supplementary Figure S3N, O). Taken together, these data suggest that CST does not limit telomerase action by simple competition for

the TPP1 telomerase binding site or by disrupting TPP1-POT1/TPP1-TIN2 association at telomeres.

Coats plus patient mutations in CTC1 OB-B weakens association with TPP1 and reduces ability to terminate telomerase

Given that the CTC1-ΔB mutation caused a deficiency in telomerase termination that results in telomere overextension, we wondered whether a similar phenotype would occur with Coats plus patient mutations that fall within the CTC1 OB-B domain. To test for this, we generated constructs to express two known OB-B patient mutations: A227V and V259M (Figure 5A) (36,56). As before, a nuclear localization sequence (NLS) was added to the N-terminus of each mutant to eliminate the previously reported defects in nuclear localization (38). The mutants were then transiently expressed in HEK293T cells or stably expressed in the *CTC1*$^{F/F}$ HCT116 cells (Supplementary Figure S1B).

Consistent with previous reports (38), EMSAs using purified protein complexes from HEK293T cells showed that both of the point mutants bound to telomeric DNA as well as wide-type CST (Supplementary Figure S4A, B). Co-immunoprecipitation experiments using extracts from HEK293T cells expressing either A227V or V259M indicated impaired CST interaction with Pol α (Figure 5B and Supplementary Figure S4C), despite neither of these residues being in close proximity to the Pol α interaction surface as seen in recent cryo-EM structures of CST-Pol α (Supplementary Figure S4D) (48,50). However, when A227V or V259M were expressed in *CTC1*$^{F/F}$ cells, both mutants prevented G-overhang elongation after endogenous CTC1 knockout (Figure 5C, D). This finding again suggests that stable interaction with Pol α may not be required for CST to function in C-strand fill-in.

Interestingly, the two mutants differed in their association with TPP1. Co-immunoprecipitation assays revealed that A227V caused only a slight (12%) reduction in CTC1-TPP1 interaction, while V259M caused a much larger reduction (51%) (Figure 5E and Supplementary Figure S4E, F). The reduced TPP-interaction caused by V259M mutation was also confirmed by the *in vitro* pull down (Supplementary Figure S4G). These different affinities for TPP1 suggest that the two mutants might differ in their ability to regulate telomerase localization to telomeres and limit telomere elongation. Indeed, when IF-FISH was used to monitor telomerase localization to telomeres in *CTC1*$^{-/-}$ cells expressing one or other mutant, the ability of the mutant to rescue the increase in TERC positive foci caused by CTC1 loss correlated with the ability of the mutant to interact with TPP1. Cells expressing V259M and ΔB had the same high level of telomere localized telomerase such that on average, 66% of V259M expressing cells and 70% of ΔB expressing cells showing >3 TERC-positive telomere foci. In contrast, cells expressing the A227V mutant showed reduced telomere localized TERC with only 49% of cells having >3 TERC-positive telomere foci, a level that is similar to that observed in cells expressing WT CTC1 where 50% of cells had >3 positive foci. (Figure 5F and Supplementary Figure S4H, I).

When we examined the effect of the A227V and V259M on TRF length (Figure 5G and Supplementary Figure S4J) we found that only V259 expressing cells caused TRF elongation (∼0.5 kb in 2 weeks). The telomere overextension caused by V259M expression was confirmed by Q-FISH (Figure 5H). It is notable that the lack of TRF elongation in A227V expressing cells was consistent with the lack of excess telomerase accumulation at telomeres (Figure 5F) and tracked with only a small decrease in TPP1 interaction (12%). In contrast, V259M and ΔB showed a similarly large decrease in TPP1 interaction (51% and 44%, respectively), similar accumulation of excess telomerase at telomeres and similar telomere elongation. These results highlight the importance of the TPP1-CTC1 interaction in telomerase regulation and provide strong evidence that the interaction between the CTC1 OB-B domain and TPP1 is essential for CST to terminate telomerase action.

DISCUSSION

Here, we identify the OB-B domain of CTC1 as a key determinant of telomerase termination, and use OB-B domain mutations to dissect the mechanism of CST function in telomere length regulation. To discover the loss of function of CTC1 mutants, we expressed each mutant in *CTC1* conditional knockout HCT116 cells and examined whether it rescues the phenotypes causing by *CTC1*$^{-/-}$. Using this system, we show that deletion of the CTC1 OB-B domain generates a separation of function mutant that still forms a complex with STN1-TEN1 (Figure 1B) and is able to promote C-strand fill-in (Figure 2B, C) such that expression of CTC1-ΔB in *CTC1*$^{-/-}$ cells prevents telomere shortening (Figure 3A). However, the OB-B deletion decreases CST binding affinity for ssDNA (Figure 1 and Supplementary Figure S1) and expression of CTC1-ΔB in *CTC1*$^{-/-}$ cells results in accumulation of telomerase at telomeres and progressive telomere elongation (Figure 3 and Supplementary Figure S2), indicating a failure to limit telomerase activity.

To better understand the mechanism of telomerase regulation by CST, we examined how the ΔB mutation affected CST and telomerase interactions with shelterin components. We show that the level of telomerase association with its shelterin interaction partners, TPP1, POT1 and TIN2, is unaffected by overexpression of CTC1-ΔB or CTC1-WT, indicating that CST is unlikely to function by disrupting these associations (Figure 4 and Supplementary Figure S3). However, the ΔB mutation greatly decreased CST interaction with TPP1 (Figure 4A, B). This decrease in CTC1-TPP1 interaction was also seen with point mutations in the CTC1 OB-B domain that cause Coats plus (A227V and V259M) (Figure 5E). Moreover, the amount of telomere elongation and telomere associated telomerase was correlated with the observed level of TPP1 interaction, with the V259M mutation, which caused the larger decrease in TPP1 interaction, leading to the higher levels of telomerase at telomeres and progressive telomere elongation in *CTC1*$^{-/-}$ cells compared to the A227V mutant, which exhibited only a minor decrease in TPP1 interaction (Figure 5E-G and Supplementary Figure S4C, D). Thus, our results point to the TPP1-CTC1 OB-B domain interaction as being key to telomerase termination.

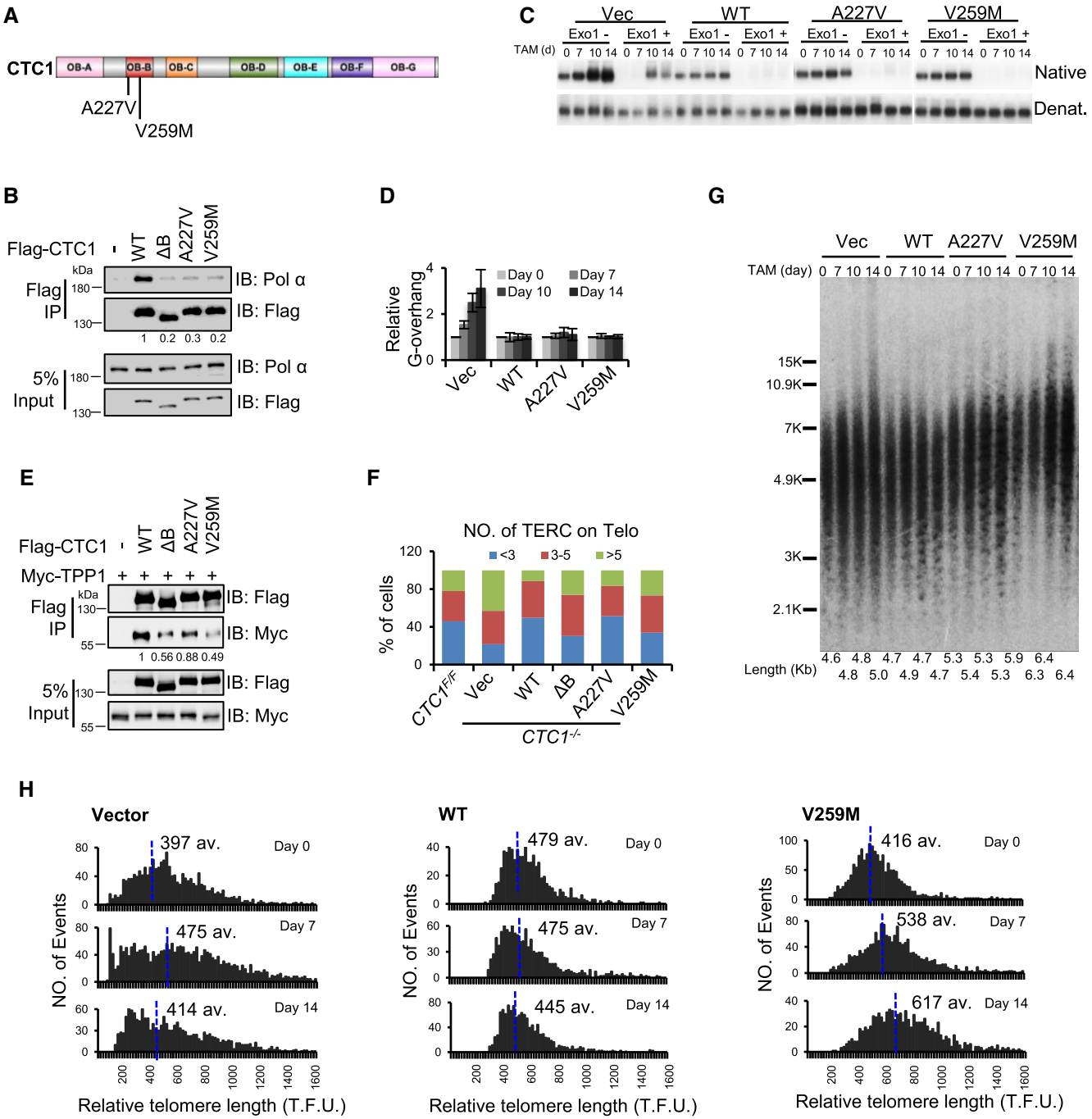

Figure 5. Coats plus patient mutation in CTC1 OB-B have weakened association with TPP1 and reduced ability to terminate telomerase. (**A**) Cartoon showing Coats plus patient mutations sites, A227V and V259M on CTC1 OB-B. (**B**) Immunoprecipitation of Flag-tagged CTC1 WT or mutants with Pol α using extracts from HEK293T. Numbers show the quantification of the amount of Pol α immunoprecipitated by WT or mutant CTC1. $N = 3$ independent experiments. (**C**, **D**) G-overhang abundance was analyzed by in-gel hybridization in *CTC1* conditional knockout cells with WT or mutated CTC1 expression following various times of TAM treatment. (C) Gels showing hybridization of TAA$(C_3TA_2)_3$ probe to genomic DNA treated with/without Exo1. (D) Quantification of relative G-overhang abundance in (C). Error bars indicate mean ± S.E.M., $n = 3$ independent experiments. (**E**) Immunoprecipitation of Flag-tagged WT or mutant CTC1 with Myc-TPP1. Numbers show the quantification of the amount of TPP1 immunoprecipitated by WT or mutant CTC1. $N = 3$ independent experiments. (**F**) Quantification of cells with TERC-telomere co-localization (The sum of three independent experiments). *CTC1* conditional knockout cells expressing WT or mutant CTC1 were treated with TAM for 7 days. >200 cells quantified per sample. (**G**) Southern blots showing TRFs in *CTC1* conditional knockout cells expressing empty vector, CTC1 WT, A227V or V259M treated with TAM for the indicated times. The gel was hybridized with ^{32}P-labeled $(TA_2C_3)_3$ G-strand probe. Mean telomere length is indicated below each lane. (**H**) Analysis of telomere length by Q-FISH *CTC*$^{-/-}$ cells with vector, CTC1-WT or CTC1-V259M expressing. Metaphase spreads were hybridized with $(C_3TA_2)_3$ G-strand probe. Histograms show distribution of relative telomere lengths expressed as fluorescence intensity (TFU, telomere fluorescence unit). A minimum of 100 TFU was set as the cut-off. av.; median value, also shown by blue line. >2000 telomeres quantified per sample.

Because the nuclear localization of CST is dependent on its interaction with Pol α, the CTC1 from Coats Plus patients with the A227V or V259M mutation is unable to enter the nucleus (38). This loss of nuclear CST in turn causes telomere shortening. In this study, we added an NLS to the protein and we note that the resulting nuclear localization of the mutant protein prevented telomere shortening, and in the case of V259M caused telomere elongation. While this stabilization/elongation of telomere length does not mimic the situation in patients, addition of the NLS was key to uncovering the importance of CTC1-TPP1 interaction. To investigate the role of CTC1-TPP1 interaction in other diseases, we used the Cancer Genome Atlas to identify cancer-associated mutations in the TID domain of TPP1, which we showed is necessary for stable CST-TPP1 interaction. A total of 10 different mutations were found in TPP1 TID domain from TCGA database (57). When we then expressed these TPP1 mutations and monitored interaction of the mutant TPP1 with CST we found that 5 out of the 10 mutants had reduced association with CTC1 (Supplementary Figure S4K). This finding suggests that disruption of the CTC1-TPP1 interaction may contribute to diseases beyond Coats Plus, including some cancers.

In initial studies of telomerase termination, Chen *et al.* found that the localization of CST on telomeres increases during S phase and peaks at S/G2, but the increase depends on the presence of active telomerase. This finding implied that CST acts after telomerase-dependent extension of the telomeric ssDNA (16), leading to the suggestion that CST terminates telomerase action by competing for binding sites on the G-overhang. Recent *in vitro* studies showed that CST cannot displace telomerase while the enzyme is elongating a DNA substrate, but it can compete with telomerase for free DNA, thus sequestering the substrate and preventing it from being extended (33). Hence, one way for CST to terminate telomerase activity *in vivo* would be by binding the G-overhang to prevent enzyme re-association when telomerase dissociates after its initial round of processive DNA synthesis (17,33).

However, our past (34) and present studies of DNA binding by CTC1-STN1 (CS) and $C_{\Delta B}ST$ complexes versus the effect of CS and $C_{\Delta B}ST$ on telomerase regulation indicate that simple competition between telomerase and CST for G-overhang binding may not be sufficient for telomerase termination. Although CS complexes bind ssDNA with significantly lower affinity than $C_{\Delta B}ST$, unlike CTC1-ΔB expressing cells, *TEN1*$^{-/-}$ cells (which contain only CS complexes (34)) remain competent to prevent telomere elongation. The realization that the ability to terminate telomerase does not simply track with CST (or CS) DNA binding affinity led us to explore the role of CTC1-TPP1 interaction in telomerase termination by analyzing the effect of CTC1 on the TPP1-POT1 protein association network.

Our analysis confirmed previous studies indicating that CST is unlikely to disrupt telomerase binding to POT1-TPP1 because, based on our findings, CST appears to interact with the TPP1 TID and RD domains rather than to OB domain (Figure 4F and H) (10,51). Moreover, TPP1 and telomerase remain associated when CST levels are increased and POT1-TPP1 telomere association is unchanged (Figure 4E and Supplementary Figure S3). In light of these findings, one model for how CST might limit telomerase action is that the TPP1-CTC1 interaction allows CST to cover the terminus of the extended G-overhang so that telomerase cannot re-bind the overhang or add additional nucleotides. Another possibility is that the TPP1-CTC1 interaction regulates telomerase via post-translational modification as occurs in yeast. In budding yeast, SUMOylation of Cdc13 (the homolog of human CTC1) is required to terminate telomerase by enhancing the interaction with Stn1/Ten1 (58). In fission yeast SUMOylation of Tpz1 (the homolog of human TPP1) enhances Tpz1-Stn1 interaction to enable release of telomerase from the telomere (59). Although the phosphorylation of human TPP1 is known to be important for telomerase recruitment (52,60), our preliminary data suggest CST does not promote TPP1 dephosphorylation and thus telomerase termination (Figure 4D and data not shown). However, it remains to be determined whether telomerase termination in humans is regulated by SUMOylation.

It is notable that the A227V and V259M Coats plus mutations exhibit greatly reduced interaction with DNA Pol α but yet fully rescue the deficiency in C-strand synthesis when expressed in *CTC1*$^{-/-}$ cells, while the CTC1-ΔB mutation with similar Pol α interaction but weaker ssDNA binding affinity shows a partial rescue. These data demonstrate that the role of CST in C-strand synthesis goes beyond simple recruitment of Pol α. This concept is reinforced by our prior finding that CTC1-STN1 (CS) complexes remain able to bind Pol α, but *TEN1*$^{-/-}$ cells are unable to support C-strand synthesis (34). Interestingly, binding of CS complexes to telomeric DNA is highly unstable with the complexes showing rapid disassociation and rebinding. It therefore appears that for C-strand synthesis to occur, the dynamics of CST binding to ssDNA equals, or possibly exceeds, the importance of CST interaction with Pol α. A likely reason for the importance of CST DNA binding dynamics stems from its RPA-like mode of binding to DNA via multiple OB-folds (44). Similar to RPA, CST likely engages and displaces ssDNA-binding proteins through the dynamic association and re-association of individual OB folds from the DNA. If CST uses this strategy to engage Pol α on the G-overhang, appropriate telomeric DNA binding by CST may be essential for C-strand fill-in. While stable interaction with Pol α likely helps recruit Pol α to the telomere, this appears to be insufficient to engage Pol α on the DNA. Based on this model, we surmise that although $C_{\Delta B}ST$ has reduced affinity for ssDNA, the overall binding dynamics are sufficiently normal for $C_{\Delta B}ST$ to engage Pol α on the G-overhang. However, removal of TEN1 results in such unstable DNA binding that the remaining CS complex is no longer competent to engage Pol α.

Based on our current findings and previous studies, we propose a model for the interplay between CST, TPP1-POT1, telomerase and Pol α during telomere replication (Figure 6A). Initially telomerase is recruited to the telomere by TPP1-POT1. The first round of telomerase extension then generates an elongated G-overhang which provides CST with space to bind. The bound CST interacts

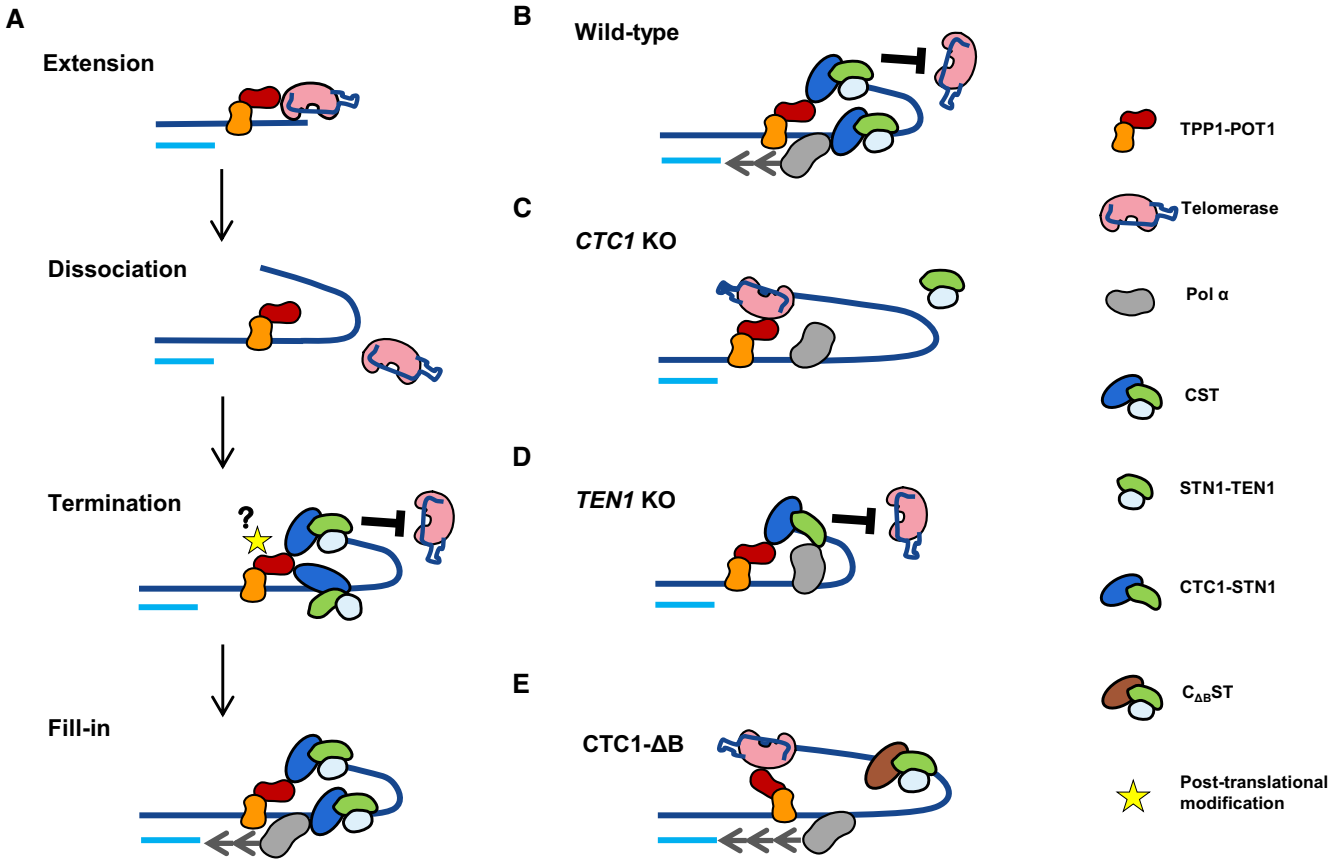

Figure 6. Model for the roles of CST in telomerase regulation and C-strand fill-in. (**A**) Telomerase is recruited by TPP1-POT1, elongates G-strand, and is released from the telomere after the first round of extension. CST then binds to the newly extended G-overhang, prevents the second round of telomerase binding by interacting with TPP1, and engages Pol α on the overhang to enable C-strand fill-in. (**B**) Wild-type CST functions in both telomerase inhibition and C-strand fill-in. (**C**) *CTC1*$^{-/-}$ cells fail to prevent G-strand overextension by telomerase and are unable to engage Pol α for C-strand fill-in. (**D**) In *TEN1*$^{-/-}$ cells, CTC1-STN1 binds to the newly extended G-strand and prevents the second-round binding of telomerase by interacting with TPP1 but is unable to engage Pol α for C-strand fill-in. (**E**) In CTC1-ΔB expressing cells, $C_{\Delta B}ST$ binds to the newly extended G-strand and engages Pol α for C-strand fill-in but fails to prevent telomerase overextension due to loss of interaction with TPP1-POT1.

with TPP1-POT1 and this interaction either enables CST to block the 3' terminus of the overhang or allows a post-translational modification of one or more telomere proteins, thus preventing a second round of telomerase extension. The dynamic nature of CST binding to DNA also allows CST to engage Pol α on the overhang thus facilitating C-strand fill-in. As a result, wild-type CST functions in both telomerase termination and C-strand fill-in (Figure 6B) while loss of CTC1 causes failure of both processes with resulting G-strand overextension and C-strand shortening (Figure 6C). In *TEN1*$^{-/-}$ cells, the residual CS complexes have normal TPP1 interaction but unstable ssDNA binding. The TPP1 interaction allows the CS complex to terminate telomerase but the altered DNA binding leaves it unable to engage Pol α. The resulting failure of C-strand fill-in leads to shortening of the telomeric dsDNA (Figure 6D). In contrast, $C_{\Delta B}ST$ has a weakened interaction with Pol α, TPP1 and binding affinity to telomeric DNA rendering the complex unable to prevent telomerase overextension. However, the DNA binding dynamics of $C_{\Delta B}ST$ are sufficient for it to engage Pol α on the G-overhang for C-strand fill-in. As a result, the extended overhangs are converted to dsDNA, causing net telomere growth (Figure 6E).

DATA AVAILABILITY

The data underlying this article are available in the article and in its online supplementary material.

SUPPLEMENTARY DATA

Supplementary Data are available at NAR Online.

ACKNOWLEDGEMENTS

We would like to thank Wenting Jiang for assistance with cell sorting, Wenjie Huang for microcopy technical support, and other members in the lab for discussion and suggestions.

FUNDING

National Natural Science Foundation of China (NSFC) [31900521, 81971305 to X.F., 82001589 to Z.L.]; Guangdong Basic and Applied Basic Research Foundation [2019A1515110832 to Z.L., 2020A1515110044 to H.W.]; China Postdoctoral Science Foundation [2021M693637 to H.W.]; NSFC [32001063 to Y.C.]; National Institutes of

Health [RO1 GM041803 to C.M.P.]. Funding for open access charge: National Natural Science Foundation of China (NSFC).
Conflict of interest statement. None declared.

REFERENCES

1. Blackburn,E.H., Epel,E.S. and Lin,J. (2015) Human telomere biology: a contributory and interactive factor in aging, disease risks, and protection. *Science*, **350**, 1193–1198.
2. Jain,D. and Cooper,J.P. (2010) Telomeric strategies: means to an end. *Annu. Rev. Genet.*, **44**, 243–269.
3. Zakian,V.A. (2012) Telomeres: the beginnings and ends of eukaryotic chromosomes. *Exp. Cell. Res.*, **318**, 1456–1460.
4. Chakravarti,D., LaBella,K.A. and DePinho,R.A. (2021) Telomeres: history, health, and hallmarks of aging. *Cell*, **184**, 306–322.
5. Penev,A., Markiewicz-Potoczny,M., Sfeir,A. and Lazzerini Denchi,E. (2022) Stem cells at odds with telomere maintenance and protection. *Trends Cell Biol.*, **32**, 527–536.
6. Shay,J.W. and Wright,W.E. (2019) Telomeres and telomerase: three decades of progress. *Nat. Rev. Genet.*, **20**, 299–309.
7. Nassour,J., Schmidt,T.T. and Karlseder,J. (2021) Telomeres and Cancer: resolving the Paradox. *Annu Rev Cancer Biol*, **5**, 59–77.
8. Roake,C.M. and Artandi,S.E. (2020) Regulation of human telomerase in homeostasis and disease. *Nat. Rev. Mol. Cell Biol.*, **21**, 384–397.
9. Zhao,Y., Sfeir,A.J., Zou,Y., Buseman,C.M., Chow,T.T., Shay,J.W. and Wright,W.E. (2009) Telomere extension occurs at most chromosome ends and is uncoupled from fill-in in human cancer cells. *Cell*, **138**, 463–475.
10. Dai,X., Huang,C., Bhusari,A., Sampathi,S., Schubert,K. and Chai,W. (2010) Molecular steps of G-overhang generation at human telomeres and its function in chromosome end protection. *EMBO J.*, **29**, 2788–2801.
11. Lim,C.J. and Cech,T.R. (2021) Shaping human telomeres: from shelterin and CST complexes to telomeric chromatin organization. *Nat. Rev. Mol. Cell Biol.*, **22**, 283–298.
12. de Lange,T. (2018) Shelterin-mediated telomere protection. *Annu. Rev. Genet.*, **52**, 223–247.
13. Kim,H., Li,F., He,Q., Deng,T., Xu,J., Jin,F., Coarfa,C., Putluri,N., Liu,D. and Songyang,Z. (2017) Systematic analysis of human telomeric dysfunction using inducible telosome/shelterin CRISPR/Cas9 knockout cells. *Cell Discov.*, **3**, 17034.
14. Miyake,Y., Nakamura,M., Nabetani,A., Shimamura,S., Tamura,M., Yonehara,S., Saito,M. and Ishikawa,F. (2009) RPA-like mammalian Ctc1-Stn1-Ten1 complex binds to single-stranded DNA and protects telomeres independently of the Pot1 pathway. *Mol. Cell*, **36**, 193–206.
15. Surovtseva,Y.V., Churikov,D., Boltz,K.A., Song,X., Lamb,J.C., Warrington,R., Leehy,K., Heacock,M., Price,C.M. and Shippen,D.E. (2009) Conserved telomere maintenance component 1 interacts with STN1 and maintains chromosome ends in higher eukaryotes. *Mol. Cell*, **36**, 207–218.
16. Chen,L.Y., Redon,S. and Lingner,J. (2012) The human CST complex is a terminator of telomerase activity. *Nature*, **488**, 540–544.
17. Zhao,Y., Abreu,E., Kim,J., Stadler,G., Eskiocak,U., Terns,M.P., Terns,R.M., Shay,J.W. and Wright,W.E. (2011) Processive and distributive extension of human telomeres by telomerase under homeostatic and nonequilibrium conditions. *Mol. Cell*, **42**, 297–307.
18. Wang,F., Podell,E.R., Zaug,A.J., Yang,Y., Baciu,P., Cech,T.R. and Lei,M. (2007) The POT1-TPP1 telomere complex is a telomerase processivity factor. *Nature*, **445**, 506–510.
19. Xin,H., Liu,D., Wan,M., Safari,A., Kim,H., Sun,W., O'Connor,M.S. and Songyang,Z. (2007) TPP1 is a homologue of ciliate TEBP-beta and interacts with POT1 to recruit telomerase. *Nature*, **445**, 559–562.
20. Zhong,F.L., Batista,L.F., Freund,A., Pech,M.F., Venteicher,A.S. and Artandi,S.E. (2012) TPP1 OB-fold domain controls telomere maintenance by recruiting telomerase to chromosome ends. *Cell*, **150**, 481–494.
21. Abreu,E., Aritonovska,E., Reichenbach,P., Cristofari,G., Culp,B., Terns,R.M., Lingner,J. and Terns,M.P. (2010) TIN2-tethered TPP1 recruits human telomerase to telomeres in vivo. *Mol. Cell. Biol.*, **30**, 2971–2982.
22. Nandakumar,J., Bell,C.F., Weidenfeld,I., Zaug,A.J., Leinwand,L.A. and Cech,T.R. (2012) The TEL patch of telomere protein TPP1 mediates telomerase recruitment and processivity. *Nature*, **492**, 285–289.
23. Chu,T.W., D'Souza,Y. and Autexier,C. (2016) The insertion in fingers domain in human telomerase can mediate enzyme processivity and telomerase recruitment to telomeres in a TPP1-dependent manner. *Mol. Cell. Biol.*, **36**, 210–222.
24. Zaug,A.J., Podell,E.R., Nandakumar,J. and Cech,T.R. (2010) Functional interaction between telomere protein TPP1 and telomerase. *Genes Dev.*, **24**, 613–622.
25. Latrick,C.M. and Cech,T.R. (2010) POT1-TPP1 enhances telomerase processivity by slowing primer dissociation and aiding translocation. *EMBO J.*, **29**, 924–933.
26. Sekne,Z., Ghanim,G.E., van Roon,A.M. and Nguyen,T.H.D. (2022) Structural basis of human telomerase recruitment by TPP1-POT1. *Science*, **375**, 1173–1176.
27. Hwang,H., Buncher,N., Opresko,P.L. and Myong,S. (2012) POT1-TPP1 regulates telomeric overhang structural dynamics. *Structure*, **20**, 1872–1880.
28. Frank,A.K., Tran,D.C., Qu,R.W., Stohr,B.A., Segal,D.J. and Xu,L. (2015) The shelterin TIN2 subunit mediates recruitment of telomerase to telomeres. *PLoS Genet.*, **11**, e1005410.
29. Pike,A.M., Strong,M.A., Ouyang,J.P.T. and Greider,C.W. (2019) TIN2 functions with TPP1/POT1 to stimulate telomerase processivity. *Mol. Cell. Biol.*, **39**, e00593-18.
30. Lim,C.J., Zaug,A.J., Kim,H.J. and Cech,T.R. (2017) Reconstitution of human shelterin complexes reveals unexpected stoichiometry and dual pathways to enhance telomerase processivity. *Nat. Commun.*, **8**, 1075.
31. Huang,C., Dai,X. and Chai,W. (2012) Human Stn1 protects telomere integrity by promoting efficient lagging-strand synthesis at telomeres and mediating C-strand fill-in. *Cell Res.*, **22**, 1681–1695.
32. Feng,X., Hsu,S.J., Kasbek,C., Chaiken,M. and Price,C.M. (2017) CTC1-mediated C-strand fill-in is an essential step in telomere length maintenance. *Nucleic Acids Res.*, **45**, 4281–4293.
33. Zaug,A.J., Lim,C.J., Olson,C.L., Carilli,M.T., Goodrich,K.J., Wuttke,D.S. and Cech,T.R. (2021) CST does not evict elongating telomerase but prevents initiation by ssDNA binding. *Nucleic Acids Res.*, **49**, 11653–11665.
34. Feng,X., Hsu,S.J., Bhattacharjee,A., Wang,Y., Diao,J. and Price,C.M. (2018) CTC1-STN1 terminates telomerase while STN1-TEN1 enables C-strand synthesis during telomere replication in colon cancer cells. *Nat. Commun.*, **9**, 2827.
35. Lim,C.J., Barbour,A.T., Zaug,A.J., Goodrich,K.J., McKay,A.E., Wuttke,D.S. and Cech,T.R. (2020) The structure of human CST reveals a decameric assembly bound to telomeric DNA. *Science*, **368**, 1081–1085.
36. Anderson,B.H., Kasher,P.R., Mayer,J., Szynkiewicz,M., Jenkinson,E.M., Bhaskar,S.S., Urquhart,J.E., Daly,S.B., Dickerson,J.E., O'Sullivan,J. *et al.* (2012) Mutations in CTC1, encoding conserved telomere maintenance component 1, cause Coats plus. *Nat. Genet.*, **44**, 338–342.
37. Gu,P. and Chang,S. (2013) Functional characterization of human CTC1 mutations reveals novel mechanisms responsible for the pathogenesis of the telomere disease Coats plus. *Aging Cell*, **12**, 1100–1109.
38. Chen,L.Y., Majerska,J. and Lingner,J. (2013) Molecular basis of telomere syndrome caused by CTC1 mutations. *Genes Dev.*, **27**, 2099–2108.
39. Gu,P., Jia,S., Takasugi,T., Smith,E., Nandakumar,J., Hendrickson,E. and Chang,S. (2018) CTC1-STN1 coordinates G- and C-strand synthesis to regulate telomere length. *Aging Cell*, **17**, e12783.
40. Wang,Y. and Chai,W. (2018) Pathogenic CTC1 mutations cause global genome instabilities under replication stress. *Nucleic Acids Res.*, **46**, 3981–3992.
41. Bhattacharjee,A., Stewart,J., Chaiken,M. and Price,C.M. (2016) STN1 OB fold mutation alters DNA binding and affects selective aspects of CST function. *PLos Genet.*, **12**, e1006342.
42. Chen,R. and Wold,M.S. (2014) Replication protein A: single-stranded DNA's first responder: dynamic DNA-interactions allow replication protein A to direct single-strand DNA intermediates into different pathways for synthesis or repair. *Bioessays*, **36**, 1156–1161.

43. Feng,X., Luo,Z., Jiang,S., Li,F., Han,X., Hu,Y., Wang,D., Zhao,Y., Ma,W., Liu,D. *et al.* (2013) The telomere-associated homeobox-containing protein TAH1/HMBOX1 participates in telomere maintenance in ALT cells. *J. Cell Sci.*, **126**, 3982–3989.
44. Bhattacharjee,A., Wang,Y., Diao,J. and Price,C.M. (2017) Dynamic DNA binding, junction recognition and G4 melting activity underlie the telomeric and genome-wide roles of human CST. *Nucleic Acids Res.*, **45**, 12311–12324.
45. Wang,F., Stewart,J.A., Kasbek,C., Zhao,Y., Wright,W.E. and Price,C.M. (2012) Human CST has independent functions during telomere duplex replication and C-strand fill-in. *Cell Rep.*, **2**, 1096–1103.
46. Mender,I. and Shay,J.W. (2015) Telomere restriction fragment (TRF) analysis. *Biol. Protoc.*, **5**, e1658.
47. Stewart,J.A., Wang,F., Chaiken,M.F., Kasbek,C., Chastain,P.D., Wright,W.E. and Price,C.M. (2012) Human CST promotes telomere duplex replication and general replication restart after fork stalling. *EMBO J.*, **31**, 3537–3549.
48. He,Q., Lin,X., Chavez,B.L., Agrawal,S., Lusk,B.L. and Lim,C.J. (2022) Structures of the human CST-Polalpha-primase complex bound to telomere templates. *Nature*, **608**, 826–832.
49. Sehnal,D., Bittrich,S., Deshpande,M., Svobodova,R., Berka,K., Bazgier,V., Velankar,S., Burley,S.K., Koca,J. and Rose,A.S. (2021) Mol* Viewer: modern web app for 3D visualization and analysis of large biomolecular structures. *Nucleic Acids Res.*, **49**, W431–W437.
50. Cai,S.W., Zinder,J.C., Svetlov,V., Bush,M.W., Nudler,E., Walz,T. and de Lange,T. (2022) Cryo-EM structure of the human CST-Polalpha/primase complex in a recruitment state. *Nat. Struct. Mol. Biol.*, **29**, 813–819.
51. Wan,M., Qin,J., Songyang,Z. and Liu,D. (2009) OB fold-containing protein 1 (OBFC1), a human homolog of yeast Stn1, associates with TPP1 and is implicated in telomere length regulation. *J. Biol. Chem.*, **284**, 26725–26731.
52. Zhang,Y., Chen,L.Y., Han,X., Xie,W., Kim,H., Yang,D., Liu,D. and Songyang,Z. (2013) Phosphorylation of TPP1 regulates cell cycle-dependent telomerase recruitment. *Proc. Natl. Acad. Sci. U.S.A.*, **110**, 5457–5462.
53. Liu,D., Safari,A., O'Connor,M.S., Chan,D.W., Laegeler,A., Qin,J. and Songyang,Z. (2004) PTOP interacts with POT1 and regulates its localization to telomeres. *Nat. Cell Biol.*, **6**, 673–680.
54. O'Connor,M.S., Safari,A., Xin,H., Liu,D. and Songyang,Z. (2006) A critical role for TPP1 and TIN2 interaction in high-order telomeric complex assembly. *Proc. Natl. Acad. Sci. U.S.A.*, **103**, 11874–11879.
55. Takai,K.K., Kibe,T., Donigian,J.R., Frescas,D. and de Lange,T. (2011) Telomere protection by TPP1/POT1 requires tethering to TIN2. *Mol. Cell*, **44**, 647–659.
56. Polvi,A., Linnankivi,T., Kivela,T., Herva,R., Keating,J.P., Makitie,O., Pareyson,D., Vainionpaa,L., Lahtinen,J., Hovatta,I. *et al.* (2012) Mutations in CTC1, encoding the CTS telomere maintenance complex component 1, cause cerebroretinal microangiopathy with calcifications and cysts. *Am. J. Hum. Genet.*, **90**, 540–549.
57. Luo,Z., Liu,W., Sun,P., Wang,F. and Feng,X. (2021) Pan-cancer analyses reveal regulation and clinical outcome association of the shelterin complex in cancer. *Brief Bioinform*, **22**, 1–12.
58. Hang,L.E., Liu,X., Cheung,I., Yang,Y. and Zhao,X. (2011) SUMOylation regulates telomere length homeostasis by targeting Cdc13. *Nat. Struct. Mol. Biol.*, **18**, 920–926.
59. Garg,M., Gurung,R.L., Mansoubi,S., Ahmed,J.O., Dave,A., Watts,F.Z. and Bianchi,A. (2014) Tpz1TPP1 SUMOylation reveals evolutionary conservation of SUMO-dependent Stn1 telomere association. *EMBO Rep.*, **15**, 871–877.
60. Hirai,Y., Tamura,M., Otani,J. and Ishikawa,F. (2016) NEK6-mediated phosphorylation of human TPP1 regulates telomere length through telomerase recruitment. *Genes Cells*, **21**, 874–889.